

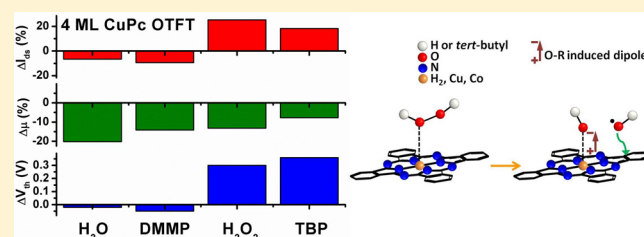
# Organic Thin-Film Transistors for Selective Hydrogen Peroxide and Organic Peroxide Vapor Detection

James E. Royer,<sup>†</sup> Erik D. Kappe,<sup>†</sup> Chengyi Zhang,<sup>†</sup> David T. Martin,<sup>‡</sup> William C. Trogler,<sup>†</sup> and Andrew C. Kummel<sup>\*,†</sup>

<sup>†</sup>Department of Chemistry and Biochemistry, <sup>‡</sup>Department of Electrical and Computer Engineering, University of California - San Diego, San Diego, La Jolla, California 92093, United States

## S Supporting Information

**ABSTRACT:** Direct selective detection of hydrogen peroxide and di-*tert*-butyl peroxide vapors was demonstrated using organic thin-film transistor (OTFT) threshold voltage shifts. Positive threshold voltage shifts are observed during peroxide vapor sensing for metal-phthalocyanine (MPc)- and naphthalocyanine (Nc)-based OTFTs. The positive threshold voltage shift observed for peroxides is not evident with nonoxidizing analytes such as dimethyl methylphosphonate (DMMP) and water. MPc and Nc OTFT sensors operating at room temperature have distinct responses in mobility and threshold voltage to peroxide vapors. The mobility changes are reversible under dry air flow, whereas positive threshold voltage shifts are reversed by counter-dosing with a polar, electron-donating analyte. The peroxide-induced threshold voltage shifts suggest an accumulation of positive charge in the MPc/Nc film. The results are consistent with a dual-response mechanism in which the peroxide molecularly chemisorbs and subsequently catalytically decomposes, forming reactive products and increasing fixed positive charge.



## 1. INTRODUCTION

Detection of vapor-phase hydrogen peroxide (VHP) has applications in the fields of biomedicine and counter-terrorism technologies. The presence of VHP in expired breath is a marker for acute respiratory failure, as well as for acute airway inflammation.<sup>1,2</sup> Sterilization of medical/pharmaceutical equipment is commonly performed with VHP at concentrations 1000 times above the permissible human exposure levels set by OSHA; therefore, *in situ* and poststerilization VHP monitoring is needed for environmental health and safety-monitoring in the workplace.<sup>3</sup> In the security sector, hydrogen peroxide- and organic peroxide-based explosives are a significant problem because they can be prepared from readily available chemicals.<sup>4,5</sup> Environmental monitoring of organic peroxides is required for analysis of harmful tropospheric air pollutants, as well as in ozone-treated drinking water.<sup>6</sup> Methods for peroxide vapor detection include chromatographic,<sup>7,8</sup> spectrophotometric,<sup>9</sup> and chemiluminescence<sup>10</sup> techniques; however, these methods require expensive and bulky instrumentation for continuous monitoring. This report describes direct selective peroxide vapor sensing using metal-phthalocyanine (MPc)- and naphthalocyanine (Nc)-based organic thin-film transistors.

Organic thin-film transistors (OTFTs) are promising candidates for selective chemical sensors because multiple chemical and electrical parameters govern sensor response. Chemically selective OTFT sensor arrays use multiple sensors with different organic thin-film semiconductor materials to develop a unique response pattern for each analyte.<sup>11–16</sup> Analyte selectivity can also be obtained using multiparameter

electrical monitoring of a single OTFT, which is sensitive to changes in mobility,  $I_{on}/I_{off}$  ratio, or threshold voltage.<sup>17–19</sup> The present study describes selective hydrogen peroxide and organic peroxide sensors based on MPc/Nc OTFT multiparameter analysis, with the focus on positive threshold voltage shifts. Detection of strong oxidant vapors using OTFTs has been previously investigated,<sup>19–23</sup> and mechanisms for oxidant-induced threshold voltage shifts in p-type OTFTs have been proposed;<sup>24,25</sup> however, the link between intermolecular interactions and sensor response remains undetermined. The analysis in this study demonstrates consistent OTFT sensor response for different peroxide vapors on vacuum-deposited MPcs and solution-deposited Ncs, thereby elucidating the chemical detection mechanism for peroxides on MPc/Nc OTFTs. The OTFT sensor response is distinct for peroxide detection and could be translated toward direct detection of organic peroxide explosives such as triacetone triperoxide (TATP) or hexamethylene triperoxide diamine (HMTD). While electrochemical sensors can easily detect aqueous hydrogen peroxide in the low ppb level,<sup>26</sup> electrochemical detection of organic peroxides requires strong acidic media to catalyze the conversion to  $H_2O_2$ .<sup>27,28</sup> The MPc/Nc OTFTs in this work operate at room temperature in air and exhibit selective sensor responses to  $H_2O_2$  and organic peroxides through positive threshold voltage shifts. The positive threshold

Received: July 11, 2012

Revised: October 15, 2012

Published: October 22, 2012

voltage shifts upon cessation of peroxide dosing are irreversible; however, counter-dosing using water vapor resets the threshold voltage shifts to the sensor baseline. The threshold voltage shifts are monitored in parallel with the OTFT mobility, which unlike the threshold voltage, is reversible at room temperature and under dry air flow. The results are consistent with the peroxide reversibly interacting with the MPc/Nc through molecular chemisorption, as well as reacting through oxidative decomposition to form reaction products with fixed charge. Mobility responses saturate quickly and are fully recoverable, consistent with molecular chemisorption, whereas positive threshold voltage shifts are dosimetric, consistent with an accumulation of positive charge in the MPc/Nc film.

## 2. MATERIALS AND METHODS

Bottom-contact thin-film transistor substrates were prepared by photolithography, using a bilayer lift-off process.<sup>29,30</sup> Interdigitated source-drain electrodes were fabricated on 100 nm thermally grown SiO<sub>2</sub>/n<sup>+</sup>Si (100) substrates (Silicon Quest). Electrodes composed of a 5 nm Ti adhesion layer and a 45 nm Au layer were deposited by electron beam evaporation under high vacuum. Deposition of the MPc was performed under ultrahigh vacuum using rates between 0.9 and 1 Å s<sup>-1</sup> with the substrates held at room temperature. All MPcs were purchased from Aldrich and purified by multiple-zone sublimation under high vacuum. 5,9,14,18,23,27,32,36-Octabutoxy-2,3-naphthalocyanine (OBNc) thin-films were spin-cast from a 2% by weight OBNc solution in toluene on OTS-treated substrates. The films had a thickness of approximately 50 nm as determined by profilometry. Synthesis of OBNc followed the literature procedure.<sup>17,31</sup>

Prior to chemical sensing, the OTFTs were electrically characterized in an optically isolated probe station using an Agilent B1500 semiconductor parameter analyzer. The devices were wire-bonded on a ceramic DIP and mounted on a printed circuit board for chemical sensing. Measurements during chemical sensing were recorded on a National Instruments PXI-6259 M-series multifunction DAQ and controlled by a custom designed LabVIEW program. Current–voltage (*I*–*V*) data for the OTFTs were analyzed every 30 or 60 s by a gate voltage (*V<sub>g</sub>*) sweep from +10 to –10 V at 4 V s<sup>-1</sup> with the drain voltage (*V<sub>ds</sub>*) held at –10 V. The drain current was monitored at a constant *V<sub>ds</sub>* = –10 V, and variable *V<sub>gs</sub>*, as indicated in the figures. The threshold voltage (*V<sub>th</sub>*) and mobility (*μ*) for each device were calculated using an automated LabVIEW program. The extracted *V<sub>th</sub>* and *μ* were obtained on the basis of a linear fit to the equation for OTFT drain current in the saturation regime (eq 1).

$$\sqrt{I_{ds}} = \sqrt{\frac{W\mu C_{ox}}{2L}} (V_{gs} - V_{th}) \quad (1)$$

For all OTFTs, the gate oxide capacitance (*C<sub>ox</sub>*) was 34.5 nF cm<sup>-2</sup>, the channel width (*W*) was 10<sup>5</sup> μm, and the channel length (*L*) was 5 μm.

Sensing experiments were performed with zero-grade air (Praxair, <2 ppm H<sub>2</sub>O, <0.02 ppm NO<sub>x</sub>) at a constant total flow of 1000 standard cubic centimeters per minute (scm). Analyte vapors were introduced into a temperature-regulated, optically isolated chamber with electrical feedthroughs, by bubbling zero-grade air through the liquid analyte. The saturated vapor was mixed with a separate dilution line within a manifold before being introduced into the sensing chamber. It

is noted that some of the H<sub>2</sub>O<sub>2</sub> may have reacted before reaching the sensors, since calibrated dosimeters showed that the H<sub>2</sub>O<sub>2</sub> present at the exit of the sensor flow system was only 25% of the concentration out of the bubbler; therefore, it is possible the sensitivities are up to 4 times greater than reported.

For safety reasons, 30% H<sub>2</sub>O<sub>2</sub> in water (Fisher) was used, and the concentration of H<sub>2</sub>O<sub>2</sub> in the vapor phase over 30% H<sub>2</sub>O<sub>2</sub> (aq) was derived from published data.<sup>32,33</sup> At 25 °C, the mole fraction of H<sub>2</sub>O<sub>2</sub> in the vapor with respect to water above the solution is only 0.01. Therefore, the vapor above a 30% solution of H<sub>2</sub>O<sub>2</sub> is approximately 1 part H<sub>2</sub>O<sub>2</sub> to 100 parts H<sub>2</sub>O.<sup>32</sup> Any H<sub>2</sub>O<sub>2</sub> dose is accompanied by a large water dose. Sensors were also dosed with di-*tert*-butyl peroxide (DTBP) or (CH<sub>3</sub>)<sub>3</sub>COOC(CH<sub>3</sub>)<sub>3</sub> (Aldrich, 98%). Vapor pressures of the DTBP from published data were used to generate concentrations of approximately 13,000 ppm using the Clausius–Clapeyron equation.<sup>34</sup>

## 3. RESULTS AND DISCUSSION

**3.1. Threshold Voltage Sensor Response.** Threshold voltage shifts in p-type OTFT sensors have been analyzed for several oxidizing and reducing agents such as NO<sub>2</sub> and NH<sub>3</sub>.<sup>19–21,23,35</sup> The analyte-induced threshold voltage shift may be positive or negative, depending on the redox properties of the analyte.<sup>19,36</sup> Organic semiconductors have electron-rich π conjugation which makes the semiconductor molecules susceptible to strong oxidants. The oxidants act as electron acceptors to either dope the semiconductor or trap charge through several possible mechanisms, including complex formation, bond cleavage, or dipole formation.<sup>19,25,37</sup> For MPc OTFTs, oxidizing species such as ozone and NO<sub>2</sub> oxidize the MPc film, resulting in an accumulation of holes in the film, increasing bulk conductivity and/or shifting *V<sub>th</sub>* to more positive values.<sup>22,23,38,39</sup>

Multiparameter sensing data for a four-monolayer (ML) CuPc OTFT exposed to water (H<sub>2</sub>O), hydrogen peroxide (H<sub>2</sub>O<sub>2</sub>), and dimethyl methylphosphonate (DMMP) with a dry air background are presented in Figure 1. Five-minute analyte pulses of 9400 ppm water (pulses 1 and 2) and 118 ppm DMMP (pulses 5 and 6) exhibit reversible, negative Δ*I<sub>ds</sub>*/*I<sub>ds0</sub>* responses. For both water and DMMP, a reversible decrease in mobility is observed, consistent with the weak electron-donating characteristics of these analytes toward CuPc.<sup>40</sup> In this study, “reversibility” is defined as Δ*I<sub>ds</sub>*/*I<sub>ds0</sub>* reverting to the baseline within a few minutes during dry air flow. Five-minute pulses of 94 ppm H<sub>2</sub>O<sub>2</sub> (pulses 3 and 4) exhibit an initial negative Δ*I<sub>ds</sub>*/*I<sub>ds0</sub>* response which inverts during dosing and becomes a positive Δ*I<sub>ds</sub>*/*I<sub>ds0</sub>* shift. The dual effect from mobility and *V<sub>th</sub>* contribute to the inversion of Δ*I<sub>ds</sub>*/*I<sub>ds0</sub>* from negative to positive during H<sub>2</sub>O<sub>2</sub> dosing.

The initial negative response on H<sub>2</sub>O<sub>2</sub> dosing could be attributed to the accompanying H<sub>2</sub>O vapor during H<sub>2</sub>O<sub>2</sub> dosing, since H<sub>2</sub>O<sub>2</sub> vapor is produced by bubbling carrier gas through a 30% H<sub>2</sub>O<sub>2</sub> (aq) solution. The vapor produced using this solution contains a 100:1 H<sub>2</sub>O/H<sub>2</sub>O<sub>2</sub> vapor ratio. Therefore, it is unknown whether the mobility decrease observed during H<sub>2</sub>O<sub>2</sub> dosing is a result of H<sub>2</sub>O<sub>2</sub> and/or H<sub>2</sub>O in the vapor mixture. The distinguishing metric for H<sub>2</sub>O<sub>2</sub> response is the positive *V<sub>th</sub>* shifts, which are not observed for H<sub>2</sub>O or DMMP. A small reversible *V<sub>th</sub>* increase occurs during the water and DMMP dosing; however, this is likely an artifact of the *I<sub>ds</sub>* – *V<sub>gs</sub>* fitting method due to the induced nonlinearity of the *I<sub>ds</sub>* – *V<sub>gs</sub>* curve during analyte dosing. An analysis of the

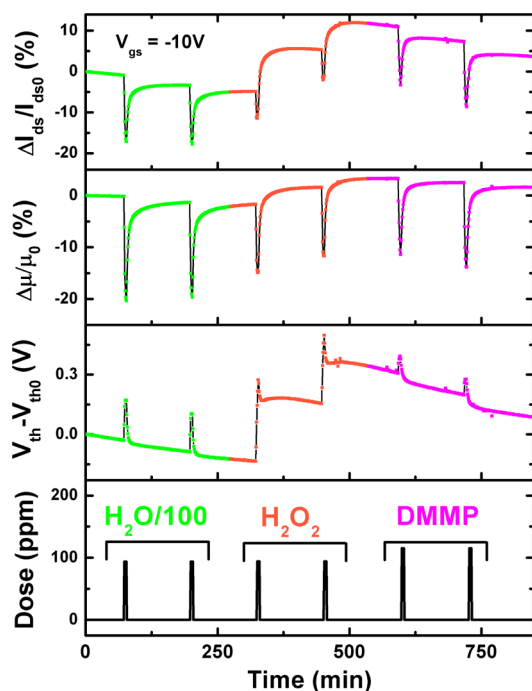


**Figure 1.** Multiparameter OTFT sensor analysis for 9400 ppm water ( $\text{H}_2\text{O}$ ) (pulses 1 and 2), 94 ppm hydrogen peroxide ( $\text{H}_2\text{O}_2$ ) (pulses 3 and 4), and 118 ppm dimethyl methylphosphonate (DMMP) (pulses 5 and 6). The  $\Delta I_{\text{ds}}/I_{\text{ds0}}$  increases for  $\text{H}_2\text{O}_2$  are due to positive  $V_{\text{th}}$  shifts, which are characteristic of an oxidant, such as  $\text{H}_2\text{O}_2$ .

$\Delta I_{\text{ds}}/I_{\text{ds0}}$  data at low  $V_{\text{gs}}$  presented in the Supporting Information [SI] (Figure S1) confirms that  $\Delta I_{\text{ds}}/I_{\text{ds0}}$  monotonically decreases for  $\text{H}_2\text{O}$  and DMMP and monotonically increases for  $\text{H}_2\text{O}_2$ . Therefore, this study focused on positive  $V_{\text{th}}$  and  $I_{\text{ds}}$  shifts as being diagnostic for peroxides.

To isolate the effects of  $\text{H}_2\text{O}_2$  vapor from those of  $\text{H}_2\text{O}$  vapor, a constant  $\text{H}_2\text{O}$  vapor background was used during  $\text{H}_2\text{O}_2$  dosing. The sensors were stabilized in a 9400 ppm  $\text{H}_2\text{O}$  vapor (30% relative humidity) ambient before  $\text{H}_2\text{O}_2$  dosing. The same  $\text{H}_2\text{O}$  vapor concentration was maintained throughout the dosing sequence by decreasing the flux of pure water during the  $\text{H}_2\text{O}_2$  pulse to compensate for the  $\text{H}_2\text{O}$  in the  $\text{H}_2\text{O}_2$  pulse (Figure 2). Using the constant  $\text{H}_2\text{O}$  vapor background technique with 4 ML CuPc OTFT sensors, there is no longer an initial decrease in  $\Delta I_{\text{ds}}/I_{\text{ds0}}$ . When monitoring the current at low  $V_{\text{gs}}$  ( $V_{\text{gs}} = -2$  V),  $\Delta I_{\text{ds}}/I_{\text{ds0}}$  is larger using a constant  $\text{H}_2\text{O}$  vapor background rather than a dry air background (Figure S1 in Supporting Information). Similarly, larger  $V_{\text{th}}$  shifts are observed when  $\text{H}_2\text{O}_2$  is dosed with a constant  $\text{H}_2\text{O}$  background. The mobility exhibits a small reversible increase (Figure 2); however, the net change in current is predominately influenced by the positive  $V_{\text{th}}$  shifts. The data is consistent with a model in which the weak binding sites on the CuPc film are nearly saturated with  $\text{H}_2\text{O}$ ; however, this is a dynamic process which could allow slow chemisorption of  $\text{H}_2\text{O}_2$  when the sites are briefly vacant. Therefore, the constant chemisorption of  $\text{H}_2\text{O}$  or  $\text{H}_2\text{O}_2$  on CuPc is consistent with small mobility changes but cumulative, irreversible  $V_{\text{th}}$  shifts. The irreversible  $V_{\text{th}}$  shifts due to  $\text{H}_2\text{O}_2$  in dry air (Figure 1) or humid air backgrounds (Figure 2), suggest that  $\text{H}_2\text{O}_2$  traps electrons as a result of a chemical reaction such as oxidation and/or a structural breakdown of the film's bulk electronic structure.

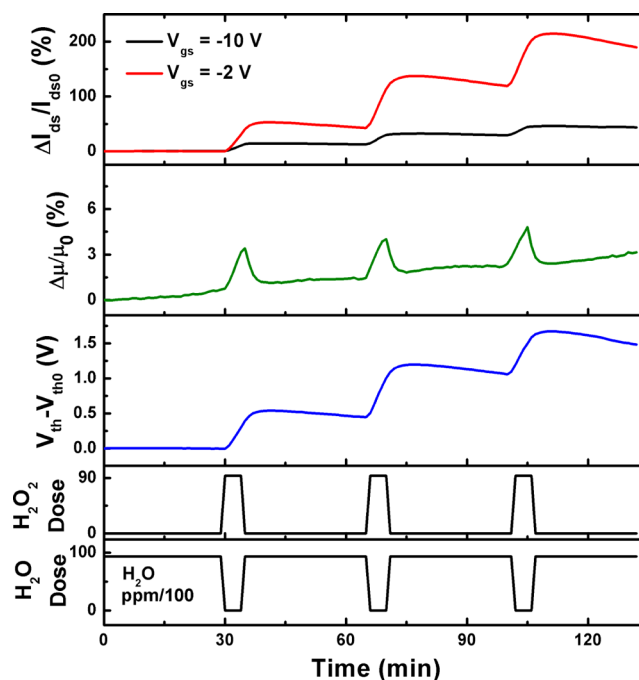


**Figure 2.** Multiparameter response of a 4 ML CuPc OTFT exposed to 5 min of a 94 ppm  $\text{H}_2\text{O}_2$  dose in a constant 9400 ppm water vapor (30% relative humidity) ambient. Both the  $\Delta I_{\text{ds}}/I_{\text{ds0}}$  and  $V_{\text{th}} - V_{\text{th0}}$  responses monotonically increase on  $\text{H}_2\text{O}_2$  dosing, consistent with isolation of the  $\text{H}_2\text{O}_2$  oxidation effect on OTFT properties.

**3.2. Dosimetric  $\text{H}_2\text{O}_2$  Sensing.** Previous reports for MPC sensors exposed to electron-donating analytes demonstrate reversible adsorption, with well-defined on and off response kinetics.<sup>40–43</sup> Conversely,  $\text{H}_2\text{O}_2$  induced  $V_{\text{th}}$  shifts in MPC OTFTs are time dependent (dosimetric) and irreversible (Figure 3). The  $V_{\text{th}}$  shift on  $\text{H}_2\text{O}_2$  exposure increases linearly with dose time for doses up to 20 min in length (Figure 3b). The mobility decrease saturates for doses longer than 5 min, similar to the response of electron-donating analytes (Figure 3a).<sup>42</sup> As explained above, the accompanying water vapor in the  $\text{H}_2\text{O}_2$  vapor dose prevents conclusive evidence for the cause of the mobility decreases. For each dose period,  $\Delta I_{\text{ds}}/I_{\text{ds0}}$  at  $V_{\text{gs}} = -10$  V has a transient decrease followed by an irreversible increase, whereas  $\Delta I_{\text{ds}}/I_{\text{ds0}}$  at  $V_{\text{gs}} = -2$  V has larger, irreversible increases. Similar to the  $V_{\text{th}}$  shifts, the percent current increases ( $\Delta I_{\text{ds}}/I_{\text{baseline}}$ ) are dosimetric at  $V_{\text{gs}} = -2$  V (Figure 3c).

This dosimetric response further supports a sensing mechanism where CuPc is oxidized by  $\text{H}_2\text{O}_2$ , which differs from the weak chemisorption events that are characteristic of most electron-donating analytes on MPCs. Chemisorbing analytes, such as water and DMMP, reversibly decrease mobility through preferential binding at the CuPc metal atom.<sup>44</sup> The preferential binding of analytes enables distinct response patterns which can improve selectivity when coupled with computer algorithms.<sup>45</sup> Similarly, the data for  $\text{H}_2\text{O}_2$  doses exhibit distinct response patterns through reversible mobility changes and irreversible  $V_{\text{th}}$  increases. Therefore, the  $\text{H}_2\text{O}_2$  doses on CuPc OTFTs exhibit response characteristics of both weak chemisorption and irreversible oxidation which could permit selectivity among other oxidizing vapors. However, the mechanism for detection remains undetermined. To determine if the peroxide induced fixed charge reaction occurs via a precursor chemisorption state, a study with organic peroxide is

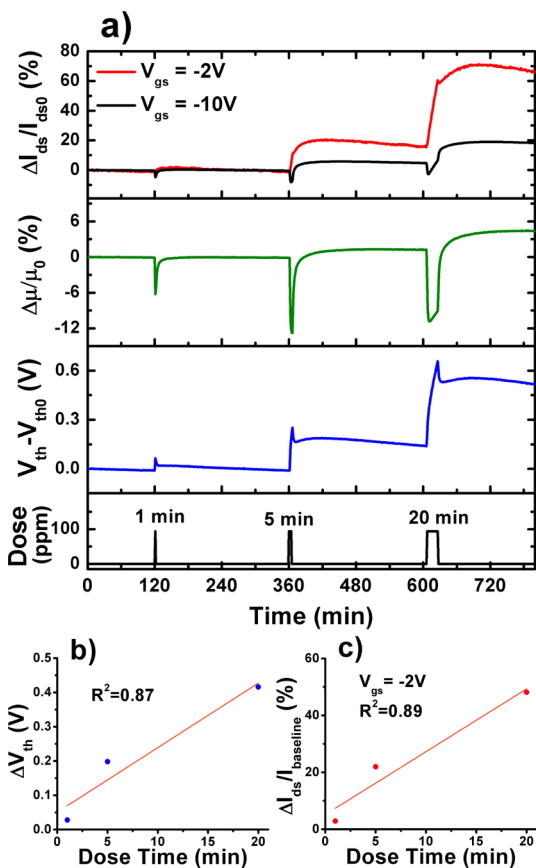


**Figure 3.** (a) Multiparameter response of a 4 ML CuPc OTFT exposed to 94 ppm  $\text{H}_2\text{O}_2$  doses for 1, 5, and 20 min. (b)  $V_{\text{th}}$  shift ( $\Delta V_{\text{th}}$ ) plotted against dose time for the response in (a). (c)  $\Delta I_{\text{ds}}/I_{\text{baseline}}$  values calculated from the un-normalized  $\Delta I_{\text{ds}}/I_{\text{ds0}}$  data at  $V_{\text{gs}} = -2$  V in (a). The  $\Delta V_{\text{th}}$  and  $\Delta I_{\text{ds}}/I_{\text{baseline}}$  values are calculated for the irreversible response as opposed to the peak-to-peak response.

required since organic peroxide can be dosed in the absence of any water vapor.

**3.3. Organic Peroxide Sensing.** An alternative approach to isolating the effects of the peroxide on MPc OTFTs was performed using the organic peroxide, di-*tert*-butyl peroxide (DTBP), which is available as a nearly pure liquid. Di-*tert*-butyl peroxide also functions as a low-hazard simulant for the explosive organic peroxides, triacetone triperoxide (TATP), and hexamethylene triperoxide diamine (HMTD). Since water is not a significant impurity, the mobility and  $V_{\text{th}}$  response can be interpreted without ambiguity since the common O–O peroxide bond induces oxidative sensing chemistry similar to that of hydrogen peroxide.

Multiparameter sensing data for a 4 ML CuPc OTFT exposed to 13000 ppm DTBP doses for 1, 3, 10, and 20 min are plotted in Figure 4a. The responses in all three parameters are similar to those obtained with  $\text{H}_2\text{O}_2$ . At  $V_{\text{gs}} = -2$  V, the  $\Delta I_{\text{ds}}/I_{\text{ds0}}$  response is irreversible and positive for all doses, whereas at  $V_{\text{gs}} = -10$  V, the  $\Delta I_{\text{ds}}/I_{\text{ds0}}$  response changes from negative to positive. These results are consistent with the positive  $V_{\text{th}}$  shifts and reversible mobility decreases observed in Figure 4a. A maximum change in mobility is obtained at approximately 3 min of dosing, similar to that obtained with  $\text{H}_2\text{O}_2$  (Figure 3a) and those shown in previous reports of chemisorbing analytes.<sup>42</sup> Conversely, the irreversible  $V_{\text{th}}$  shift increases

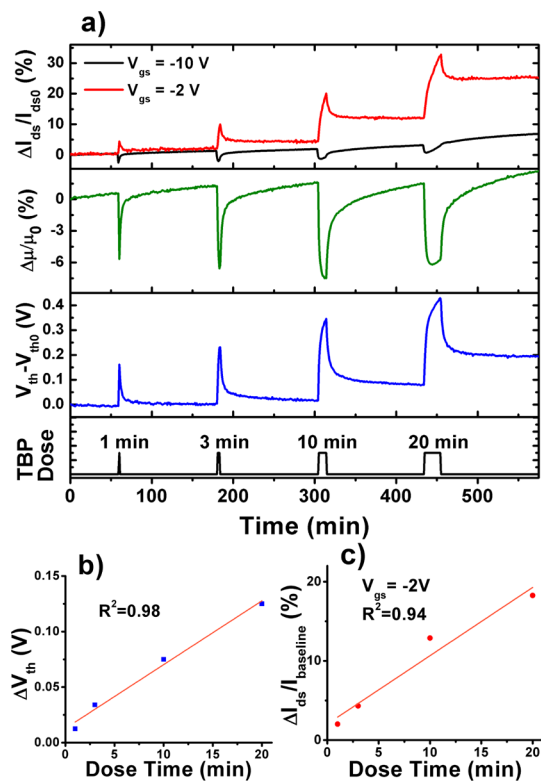


**Figure 4.** (a) Multiparameter response of a 4 ML CuPc OTFT exposed to 13000 ppm DTBP ( $((\text{CH}_3)_3\text{COOC}(\text{CH}_3)_3$ ) doses for 1, 3, 10, and 20 min. (b)  $V_{\text{th}}$  shift ( $\Delta V_{\text{th}}$ ) plotted against dose time for the response in (a). (c)  $\Delta I_{\text{ds}}/I_{\text{baseline}}$  values calculated from the un-normalized  $\Delta I_{\text{ds}}/I_{\text{ds0}}$  data in (a). The  $\Delta I_{\text{ds}}/I_{\text{baseline}}$  and  $\Delta V_{\text{th}}$  is calculated for the irreversible response as opposed to the peak-to-peak response.

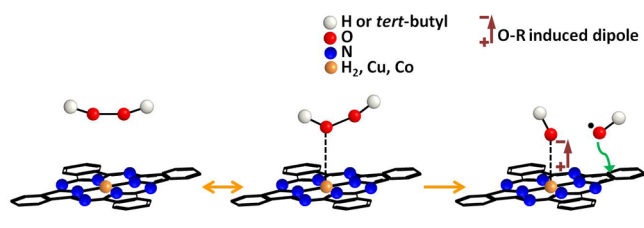
linearly with dose time (Figure 4b), as does the irreversible component of the  $\Delta I_{\text{ds}}/I_{\text{ds0}}$  response at  $V_{\text{gs}} = -2$  V (Figure 4c).

The results support a mechanism proceeding through reversible molecular chemisorption followed by CuPc oxidation and irreversible cleavage of the peroxide O–O bond. The nearly identical mobility and  $V_{\text{th}}$  responses for both DTBP and  $\text{H}_2\text{O}_2$  suggest that both peroxides undergo this chemisorption/oxidation reaction mechanism. Previous reports have attributed reversible mobility decreases to chemisorption on MPc OTFTs,<sup>43,46</sup> whereas irreversible  $V_{\text{th}}$  increases are usually attributed to induced trap states or fixed charge.<sup>38,47</sup> However, few reports have shown both reversible mobility decreases and irreversible  $V_{\text{th}}$  increases for a specific analyte.<sup>20</sup> The sensing mechanism distinguishes peroxides from nonredox analytes, which only chemisorb to the MPc through hydrogen bonding or electron donation and therefore do not break bonds.<sup>42</sup> Strong oxidants, such as chlorine or ozone, exhibit irreversible sensing but do not exhibit evidence of a detectable reversibly bound precursor.<sup>48</sup> The data for both peroxide analytes suggest that CuPc may act as a catalyst for breaking the peroxide RO–OR bond. Previous reports have demonstrated decomposition of TATP and HMTD using  $\text{Cu}^{2+}$  ions,<sup>49</sup> and many different MPcs have been reported as oxidation catalysts with peroxides.<sup>50,51</sup> Therefore, the consistency of this sensing mechanism was investigated using different MPcs, as described below.

CuPc, CoPc, and  $\text{H}_2\text{Pc}$  OTFTs were tested simultaneously *in situ* to determine the effects of different metal centers on the

threshold voltage and mobility responses. The multiparameter responses of 4 ML CuPc, CoPc, and H<sub>2</sub>Pc OTFTs exposed to 1, 3, 10, and 20 min doses of 13000 ppm DTBP are presented in Figure S2 (SI). Dosimetric behavior is observed for all MPc OTFTs. Compared to CuPc, the CoPc sensor exhibits a larger  $\Delta V_{th}$ , and a larger  $\Delta I_{ds}/I_{baseline}$ . For sensors of each material, the mobility decrease saturates for dose lengths of 3 min or longer, and the percent decrease is within a factor of 2. Similar mobility responses but different  $V_{th}$  responses between the three different MPcs are consistent with the mechanism described above for CuPc OTFTs. A schematic for the catalytic decomposition of peroxide by MPc is shown in Scheme 1.<sup>52,53</sup> The enhanced  $V_{th}$  shifts observed for CoPc may be

### Scheme 1. Model of the Catalytic Decomposition of Peroxides on MPc To Form Positive Fixed Charge



attributed to its improved catalytic properties. CoPc is often utilized as a catalyst for peroxide oxidation due to its high redox activity.<sup>50,54</sup> Therefore, the CoPc film would have a higher surface concentration of reactive O–R radicals, which should lead to irreversible oxidation reactions. The other O–R group could also remain adsorbed to the metal center, forming a fixed dipole and causing positive  $V_{th}$  shifts.

In a control experiment involving dosimetric H<sub>2</sub>O<sub>2</sub> exposures on CuPc, CoPc, and H<sub>2</sub>Pc, CoPc again demonstrated the largest  $\Delta V_{th}$  and  $\Delta I_{ds}/I_{baseline}$ , consistent with the catalytic mechanism for  $V_{th}$  shifts (Figure S3 [SI]). However, the difference in  $V_{th}$  shifts is less pronounced between CoPc and H<sub>2</sub>Pc compared to results with organic peroxide, probably due to the high reactivity of H<sub>2</sub>O<sub>2</sub> compared to organic peroxide, diminishing the difference in catalytic efficiency between CoPc and H<sub>2</sub>Pc. Note that the proposed mechanism still requires further analysis to determine the chemical nature of the surface-bound analyte redox products.

**3.4. Improved Sensor Response Using Solution-Processed OTFTs.** The dual sensor response for vacuum-deposited MPc OTFTs yields a distinct signature for peroxide vapor detection; however, these MPc OTFTs have low OTFT performance and can be unstable in ambient air. Vacuum-deposited MPcs are also incompatible with solution-processing methods which make them undesirable for large area sensor array fabrication. Spin-coated octa-butoxy naphthalocyanine (OBNc) OTFTs have demonstrated improved OTFT device characteristics and sensor performance relative to those of H<sub>2</sub>Pc OTFTs.<sup>17</sup> The OBNc OTFTs also exhibit improved air stability, which permits more stable sensor baselines.

Due to their improved stability in ambient air, OBNc OTFTs are more suitable for practical sensing applications. Therefore, the OBNc OTFTs were exposed to DTBP doses under a humid atmosphere to simulate practical sensing conditions. The multiparameter data for OBNc OTFTs exposed to 1, 3, 10, and 20 min doses of 13000 ppm DTBP under a 30% relative humidity background are presented in Figure 5a. The calculated sensor responses for  $\Delta V_{th}$  and  $\Delta I_{ds}/I_{baseline}$  are very linear ( $R^2 >$

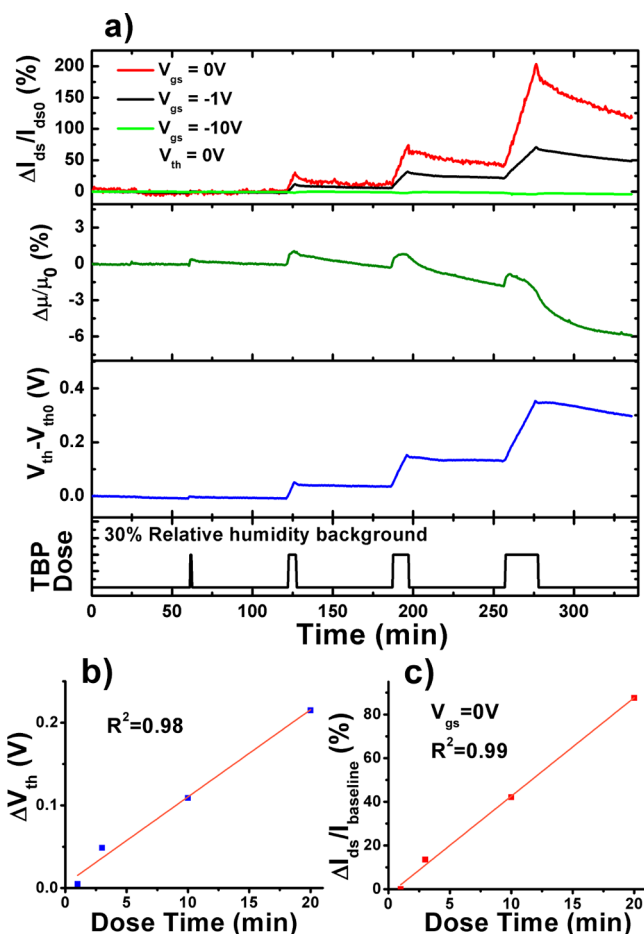


**Figure 5.** (a) Multiparameter responses of spin-coated OBNc OTFTs exposed to 13000 ppm DTBP doses for 1, 3, 10, and 20 min, with a 30% relative humidity background. (b)  $V_{th}$  shift ( $\Delta V_{th}$ ) plotted against dose time for the response in (a). (c)  $\Delta I_{ds}/I_{baseline}$  values calculated from the un-normalized  $\Delta I_{ds}/I_{ds0}$  data in (a) for  $V_{gs} = 0$  V. The large  $\Delta I_{ds}/I_{ds0}$  response is consistent with the steep subthreshold slope for OBNc OTFTs. The  $\Delta I_{ds}/I_{baseline}$  and  $\Delta V_{th}$  is calculated for the irreversible response as opposed to the peak-to-peak response.

0.98) (b and c of Figure 5), and are of similar magnitude to those with a dry air background (Figure S4 [SI]). The mobility exhibits only small reversible increases on DTBP exposure in Figure 5a, similar to the case of the 4 ML CuPc OTFT exposed to H<sub>2</sub>O<sub>2</sub> with a humid background (Figure 2). These results suggest that the background conditions, dry air or humid air, primarily influence the weaker chemisorption properties of the DTBP as opposed to the reaction which leads to fixed charge and positive shifts in  $I_{ds}$  and  $V_{th}$ . This chemisorption state could be sensitive to coadsorbates, such as water; however, the net reaction of peroxides leading to fixed positive charge is independent of the background conditions, as exhibited by the dosimetric response in all devices with and without background H<sub>2</sub>O. OBNc OTFTs exhibit a large  $\Delta I_{ds}/I_{ds0}$  response at  $V_{gs} \approx V_{th}$ , similar to the 4 ML CoPc OTFT response. The calculated  $V_{th}$  shifts are smaller for OBNc OTFTs, relative to those for CoPc OTFTs, possibly due to the lack of a central metal atom in the OBNc molecule, which prevents efficient catalytic decomposition of the peroxide.

The sensitivity and detection limit for DTBP are significantly improved in OBNc OTFTs relative to those of MPc OTFTs (Table 1). Note that the sensitivities are expressed as %

Table 1. OTFT Device Parameters and Detection Limits for DTBP<sup>a</sup>

	$\mu$ (cm <sup>2</sup> V <sup>-1</sup> s <sup>-1</sup> )	$V_{th}$ (V)	$I_{on}/I_{off}$	$S$ (V/decade)	sensitivity (% ppm <sup>-1</sup> min <sup>-1</sup> ) $\times$ 100	detection limit DTBP (ppm)
OBNC	0.003	-0.58	$6.1 \times 10^4$	0.49	0.027	0.64
	( $1. \times 10^{-4}$ )	(0.08)	( $0.8 \times 10^4$ )	(0.02)	(0.005)	
CoPc	$7.6 \times 10^{-5}$	3.5	$2.2 \times 10^2$	6.1	0.015	4.1
	( $1.8 \times 10^{-5}$ )	(0.2)	( $1.4 \times 10^2$ )	(3.0)	(0.003)	
CuPc	$2.7 \times 10^{-4}$	-0.19	$2.2 \times 10^3$	2.5	0.007	11.1
	( $0.6 \times 10^{-4}$ )	(0.22)	( $2.1 \times 10^3$ )	(0.7)	( $4 \times 10^{-4}$ )	
H <sub>2</sub> Pc	$2.2 \times 10^{-4}$	-1.6	$1.3 \times 10^3$	1.5	0.004	1230
	( $1.8 \times 10^{-4}$ )	(0.3)	( $0.9 \times 10^3$ )	(0.6)	( $4 \times 10^{-4}$ )	

<sup>a</sup>Device parameters were calculated from transfer data recorded in the dark, at room-temperature, in ambient air. The sensitivities and detection limits are calculated for DTBP doses with dry air background. Standard deviations are shown in parentheses.

ppm<sup>-1</sup> min<sup>-1</sup> since these sensors are dosimetric; therefore, the values for sensitivity do not directly compare with non-dosimetric peroxide sensors, which demonstrate saturated response within 10 min.<sup>52</sup> The detection limits were calculated on the basis of the  $\Delta I_{ds}/I_{baseline}$  percentages for 20 min doses at a signal-to-noise ratio of 3.

Since peroxide vapors reproducibly induce a positive  $V_{th}$  shift in MPC and OBNC OTFTs, it is possible to reverse the effect of peroxide on the sensors by inducing a negative  $V_{th}$  shift. It is noted that this is a chemically induced reversal and not the spontaneous reversible chemisorption observed for other strong chemisorbing analytes.<sup>42</sup> Previous work has identified polar analytes, such as water, which act as hole carrier traps in OBNC OTFTs, and cause negative  $V_{th}$  shifts.<sup>17</sup> Therefore, large water vapor doses were utilized in between DTBP doses on OBNC OTFT sensors to induce negative  $V_{th}$  shifts, and reset the  $\Delta V_{th}$  and  $\Delta I_{ds}/I_{ds0}$  to baseline. While monitoring the multiparameter OTFT response under 30% humidity, DTBP was dosed for 10 min at 13000 ppm and, subsequently, the humidity was increased to 60% for 20 min (Figure 6).

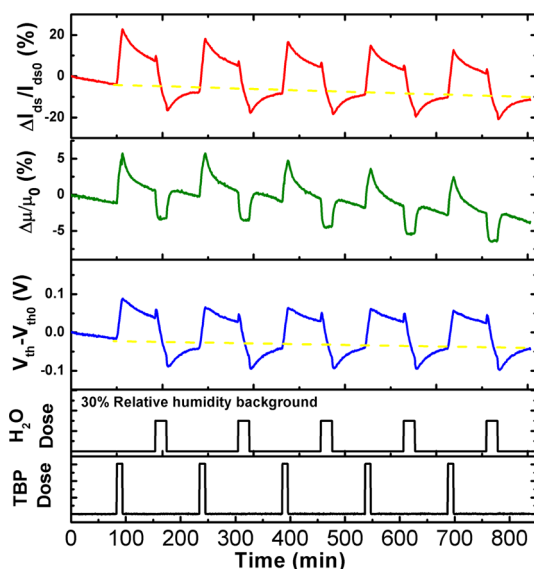


**Figure 6.** Multiparameter response for reversible DTBP sensing on OBNC OTFTs. The OBNC OTFTs were operated under 30% relative humidity and exposed to 10 min doses of 13000 ppm DTBP. The OTFTs were subsequently exposed to 20 min doses of 60% relative humidity. The peroxide induced irreversible positive shifts in  $\Delta I_{ds}/I_{ds0}$  and  $V_{th}$  can be compensated by H<sub>2</sub>O-induced irreversible negative shifts in  $\Delta I_{ds}/I_{ds0}$  and  $V_{th}$ . The dotted yellow lines are a guide to illustrate the return to baseline in  $\Delta I_{ds}/I_{ds0}$  and  $V_{th} - V_{th0}$ .

The  $\Delta I_{ds}/I_{ds0}$  response at  $V_{gs} = 0$  V illustrates the effects of positive and negative  $V_{th}$  shifts due to the peroxide and water. Although the large water doses cause some overshoot in  $\Delta I_{ds}/I_{ds0}$  and  $V_{th} - V_{th0}$ , the net effect is an irreversible negative shift which recovers to the baseline. The mobility response again demonstrates small reversible increases from the DTBP exposure and small reversible decreases from the 60% humidity exposure. The  $\Delta I_{ds}/I_{ds0}$  and  $V_{th} - V_{th0}$  panels of Figure 6 illustrate how the sensor returns to the baseline shortly after the water dose. The pattern is repeated to confirm consistent responses in the  $V_{th}$  and  $I_{ds}$  shifts.

#### 4. CONCLUSIONS

MPC- and OBNC-based OTFTs exhibit positive threshold voltage shifts on exposure to hydrogen peroxide and di-*tert*-butyl peroxide vapors. Threshold voltage analysis of peroxide vapor permits improved sensitivity and selectivity with respect to nonoxidizing analytes. MPC and OBNC OTFTs exhibit positive shifts in  $I_{ds}$  and  $V_{th}$ , which can be reversed by counter-dosing with a polar, electron-donating analyte such as water. Unlike the threshold voltage shifts, the mobility response to peroxide vapors is fully reversible in dry air flow. The dual response for peroxide-sensing suggests a mechanism in which chemisorption reversibly increases or decreases mobility, followed by redox cleavage of the peroxide bond, which induces fixed positive charge causing a positive  $V_{th}$  shift. These OTFT sensors present advantages since they can directly and selectively detect peroxide analytes due to their unique chemisorption and catalytic behavior.

#### ■ ASSOCIATED CONTENT

##### Supporting Information

Low gate voltage sensing data, and multiparameter sensing data of peroxides using CuPc, CoPc, H<sub>2</sub>Pc, and OBNC OTFTs. This material is available free of charge via the Internet at <http://pubs.acs.org>.

#### ■ AUTHOR INFORMATION

##### Corresponding Author

\*E-mail: [akummel@ucsd.edu](mailto:akummel@ucsd.edu).

##### Notes

The authors declare no competing financial interest.

#### ■ ACKNOWLEDGMENTS

Support by AFOSR STTR II Contracts FA9550-10-C-0019 and FA9550-10-C-0011 along with NSF Grant CHE-0848502 is gratefully acknowledged.

## REFERENCES

- (1) Dohlman, A. W.; Black, H. R.; Royall, J. A. *Am. Rev. Respir. Dis.* **1993**, *148*, 955.
- (2) Kietzmann, D.; Kahl, R.; Muller, M.; Buchardi, H.; Kettler, D. *Intensive Care Med.* **1993**, *19*, 78.
- (3) Park, J.; Plese, M. R.; Puskar, M. A. *AIHA (Am. Ind. Hygiene Assoc.) J.* **2003**, *64*, 360.
- (4) Wang, J. *Electroanalysis* **2007**, *19*, 415.
- (5) Armitt, D.; Zimmermann, P.; Ellis-Steinborner, S. *Rapid Commun. Mass Spectrom.* **2008**, *22*, 950.
- (6) Li, J. Z.; Dasgupta, P. K. *Anal. Chem.* **2000**, *72*, 5338.
- (7) Oxley, J. C.; Smith, J. L.; Chen, H. *Propellants Explosives Pyrotechnics* **2002**, *27*, 209.
- (8) Muller, D.; Levy, A.; Shelef, R.; Abramovich-Bar, S.; Sonenfeld, D.; Tamiri, T. *J. Forensic Sci.* **2004**, *49*, 935.
- (9) Pacheco-Londono, L. C.; Ortiz-Rivera, W.; Primera-Pedrozo, O. M.; Hernandez-Rivera, S. P. *Anal. Bioanal. Chem.* **2009**, *395*, 323.
- (10) Sanchez, J. C.; Trogler, W. C. *J. Mater. Chem.* **2008**, *18*, 5134.
- (11) Torsi, L.; Farinola, G. M.; Marinelli, F.; Tanese, M. C.; Omar, O. H.; Valli, L.; Babudri, F.; Palmisano, F.; Zambonin, P. G.; Naso, F. *Nat. Mater.* **2008**, *7*, 412.
- (12) Torsi, L.; Dodabalapur, A.; Sabbatini, L.; Zambonin, P. G. *Sens. Actuators, B* **2000**, *67*, 312.
- (13) Crone, B.; Dodabalapur, A.; Gelperin, A.; Torsi, L.; Katz, H. E.; Lovinger, A. J.; Bao, Z. *Appl. Phys. Lett.* **2001**, *78*, 2229.
- (14) Torsi, L.; Tanese, M. C.; Cioffi, N.; Gallazzi, M. C.; Sabbatini, L.; Zambonin, P. G. *Sens. Actuators, B* **2004**, *98*, 204.
- (15) Tanese, M. C.; Fine, D.; Dodabalapur, A.; Torsi, L. *Microelectron. J.* **2006**, *37*, 837.
- (16) Chang, J. B.; Liu, V.; Subramanian, V.; Sivula, K.; Luscombe, C.; Murphy, A.; Liu, J.; Frechet, J. M. J. *J. Appl. Phys.* **2006**, *100*, 014506.
- (17) Royer, J. E.; Zhang, C.; Kummel, A. C.; Trogler, W. C. *Langmuir* **2012**, *28*, 6192.
- (18) Huang, J.; Dawidczyk, T. J.; Jung, B. J.; Sun, J.; Mason, A. F.; Katz, H. E. *J. Mater. Chem.* **2010**, *20*, 2644.
- (19) Marinelli, F.; Dell'Aquila, A.; Torsi, L.; Tey, J.; Suranna, G. P.; Mastroianni, P.; Romanazzi, G.; Nobile, C. F.; Mhaisalkar, S. G.; Cioffi, N.; Palmisano, F. *Sens. Actuators, B* **2009**, *140*, 445.
- (20) Das, A.; Dost, R.; Richardson, T.; Grell, M.; Morrison, J. J.; Turner, M. L. *Adv. Mater.* **2007**, *19*, 4018.
- (21) Guillaud, G.; Simon, J.; Germain, J. P. *Coord. Chem. Rev.* **1998**, *178*, 1433.
- (22) Bouvet, M.; Leroy, A.; Simon, J.; Tournilhac, F.; Guillaud, G.; Lessnick, P.; Maillard, A.; Spirkovitch, S.; Debliquy, M.; de Haan, A.; Decroly, A. *Sens. Actuators, B* **2001**, *72*, 86.
- (23) Bouvet, M.; Guillaud, G.; Leroy, A.; Maillard, A.; Spirkovitch, S.; Tournilhac, F. G. *Sens. Actuators, B* **2001**, *73*, 63.
- (24) Northrup, J. E.; Chabiny, M. L. *Phys. Rev. B* **2003**, *68*, 041202.
- (25) Chabiny, M. L.; Street, R. A.; Northrup, J. E. *Appl. Phys. Lett.* **2007**, *90*, 123508.
- (26) Benedet, J.; Lu, D.; Cizek, K.; La Belle, J.; Wang, J. *Anal. Bioanal. Chem.* **2009**, *395*, 371–376.
- (27) Munoz, R. A. A.; Lu, D.; Cagan, A.; Wang, J. *Analyst* **2007**, *132*, 560.
- (28) Laine, D. F.; Roske, C. W.; Cheng, I. F. *Anal. Chim. Acta* **2008**, *608*, 56.
- (29) Royer, J. E.; Park, J.; Colesniuc, C.; Lee, J. S.; Gredig, T.; Lee, S.; Jin, S.; Schuller, I. K.; Trogler, W. C.; Kummel, A. C. *J. Vac. Sci. Technol. B* **2010**, *28*, CSF22.
- (30) Park, J.; Yang, R. D.; Colesniuc, C. N.; Sharoni, A.; Jin, S.; Schuller, I. K.; Trogler, W. C.; Kummel, A. C. *Appl. Phys. Lett.* **2008**, *92*, 193311.
- (31) Rihter, B. D.; Kenney, M. E.; Ford, W. E.; Rodgers, M. A. J. *J. Am. Chem. Soc.* **1993**, *115*, 8146.
- (32) Manatt, S. L.; Manatt, M. R. R. *Chem.—Eur. J.* **2004**, *10*, 6540.
- (33) Scatchard, G.; Kavanagh, G. M.; Ticknor, L. B. *J. Am. Chem. Soc.* **1952**, *74*, 3715.
- (34) Diogo, H. P.; Minas da Piedade, M. E.; Martinho Simões, J. A.; Nagano, Y. *J. Chem. Thermodynam.* **1995**, *27*, 597.
- (35) Jeong, J. W.; Lee, Y. D.; Kim, Y. M.; Park, Y. W.; Choi, J. H.; Park, T. H.; Soo, C. D.; Won, S. M.; Han, I. K.; Ju, B. K. *Sens. Actuators, B* **2010**, *146*, 40.
- (36) Pacher, P.; Lex, A.; Proschek, V.; Etschmaier, H.; Tchernychova, E.; Sezen, M.; Scherf, U.; Grogger, W.; Trimmel, G.; Slugovc, C.; Zojer, E. *Adv. Mater.* **2008**, *20*, 3143.
- (37) Andringa, A.-M.; Meijboom, J. R.; Smits, E. C. P.; Mathijssen, S. G. J.; Blom, P. W. M.; de Leeuw, D. M. *Adv. Funct. Mater.* **2011**, *21*, 100.
- (38) Park, J.; Royer, J. E.; Colesniuc, C. N.; Bohrer, F. I.; Sharoni, A.; Jin, S. H.; Schuller, I. K.; Trogler, W. C.; Kummel, A. C. *J. Appl. Phys.* **2009**, *106*, 034505.
- (39) Hu, W. P.; Liu, Y. Q.; Xu, Y.; Liu, S. G.; Zhou, S. Q.; Zhu, D. B.; Xu, B.; Bai, C. L.; Wang, C. *Thin Solid Films* **2000**, *360*, 256.
- (40) Yang, R. D.; Park, J.; Colesniuc, C. N.; Schuller, I. K.; Royer, J. E.; Trogler, W. C.; Kummel, A. C. *J. Chem. Phys.* **2009**, *130*, 164703.
- (41) Collins, R. A.; Mohammed, K. A. *J. Phys. D: Appl. Phys.* **1988**, *21*, 154.
- (42) Bohrer, F. I.; Sharoni, A.; Colesniuc, C.; Park, J.; Schuller, I. K.; Kummel, A. C.; Trogler, W. C. *J. Am. Chem. Soc.* **2007**, *129*, 5640.
- (43) Bora, M.; Schut, D.; Baldo, M. A. *Anal. Chem.* **2007**, *79*, 3298.
- (44) Tran, N. L.; Kummel, A. C. *J. Chem. Phys.* **2007**, *127*, 214702.
- (45) Bohrer, F. I.; Colesniuc, C. N.; Park, J.; Ruidiaz, M. E.; Schuller, I. K.; Kummel, A. C.; Trogler, W. C. *J. Am. Chem. Soc.* **2009**, *131*, 478.
- (46) Royer, J. E.; Lee, S.; Chen, C.; Ahn, B.; Trogler, W. C.; Kanicki, J.; Kummel, A. C. *Sens. Actuators, B* **2011**, *158*, 333.
- (47) Zhivkov, I.; Nespurek, S.; Schauer, F. *Adv. Mater. Opt. Electron.* **1999**, *9*, 175.
- (48) Azim-Araghi, M. E.; Krier, A. *Appl. Surf. Sci.* **1997**, *119*, 260.
- (49) Pentildea-Quevedo, A. J.; Figueroa, J.; Rodriguez, N.; Nieves, D.; Hernandez, N.; Rivera, R.; Mina, N.; Hernandez-Rivera, S. P. *Proc. SPIE-Int. Soc. Opt. Eng.* **2006**, *6201*, 62012D-1-11.
- (50) Sorokin, A. B.; Kudrik, E. V. *Catal. Today* **2011**, *159*, 37.
- (51) Sorokin, A. B.; Tuel, A. *Catal. Today* **2000**, *57*, 45.
- (52) Bohrer, F. I.; Colesniuc, C. N.; Park, J.; Schuller, I. K.; Kummel, A. C.; Trogler, W. C. *J. Am. Chem. Soc.* **2008**, *130*, 3712.
- (53) Gantchev, T. G.; Sharman, W. M.; van Lier, J. E. *Photochem. Photobiol.* **2003**, *77*, 469.
- (54) Paez-Mozo, E.; Gabriunas, N.; Maggi, R.; Acosta, D.; Ruiz, P.; Delmon, B. *J. Mol. Catal.* **1994**, *91*, 251.